frontiers in Environmental Science

ORIGINAL RESEARCH
published: 19 September 2018
doi: 10.3389/fenvs.2018.00093

Bacterial Extracellular Polymeric Substances Amplify Water Content Variability at the Pore Scale

*Yi-Syuan Guo[1], Jessica M. Furrer[2], Andrea L. Kadilak[1], Hector F. Hinestroza[2], Daniel J. Gage[3], Yong Ku Cho[1] and Leslie M. Shor[1,4,5]**

[1] Department of Chemical and Biomolecular Engineering, University of Connecticut, Storrs, CT, United States, [2] Department of Physics and Engineering, Benedict College, Columbia, SC, United States, [3] Department of Molecular and Cellular Biology, University of Connecticut, Storrs, CT, United States, [4] Center for Environmental Sciences & Engineering, University of Connecticut, Storrs, CT, United States, [5] School of Chemical Engineering, The University of Adelaide, Adelaide, SA, Australia

The function of microbial communities in soil is inextricably linked with the complex physical, chemical, and biological structure of the soil itself. Pore-scale water content controls the hydraulic connectivity of microbial communities and microbes' access to aqueous and gaseous substrates. In turn, soil bacteria directly influence local moisture conditions through the secretion of extracellular polymeric substances (EPS). However, the effect of a soil's physical geometry on EPS-mediated water retention is not well understood. In this study, we systematically measured the rate and extent of water evaporation from pore structures as a function of both EPS concentration and pore size. Three different chamber types were employed: (i) glass capillary tubes (1.2 mm pore diameter) to represent a uniform macropore geometry; (ii) emulated soil micromodels (pore widths ~10 to >300 μm) to represent an aggregated sandy loam pore geometry; and (iii) microfluidic capillary arrays (uniform channels 20 μm wide) to represent a uniform micropore geometry. All chambers were initially saturated with dilute EPS solutions collected from stationary-phase *Sinorhizobium meliloti* cultures and then the infiltration of air was tracked over time. In the largest chambers, EPS concentration had no effect on the extent of evaporation or on the magnitude or variability of the evaporation rate. However, in the chambers with micropore-sized physical features, EPS concentration strongly influenced rate, extent, and variability of pore water evaporation. In micropores, higher EPS concentrations enhanced water retention and led to greater variability in pore-scale water distributions. In real soil, these phenomena could act together to promote the intermediate water contents associated with productive soil systems, and more variable pore-scale water distributions could increase microbial community diversity and the resiliency of soil systems.

Keywords: extracellular polysaccharide, evaporation, micromodel, microfluidics, rhizosphere soil, soil aggregate, soil moisture

OPEN ACCESS

Edited by:
Wilfred Otten,
Cranfield University, United Kingdom

Reviewed by:
Eiko Eurya Kuramae,
Netherlands Institute of Ecology (NIOO-KNAW), Netherlands
Christophe Darnault,
Clemson University, United States

****Correspondence:***
Leslie M. Shor
LeslieShor@gmail.com

Specialty section:
This article was submitted to Soil Processes, a section of the journal Frontiers in Environmental Science

Received: *06 April 2018*
Accepted: *09 August 2018*
Published: *19 September 2018*

Citation:
Guo Y-S, Furrer JM, Kadilak AL, Hinestroza HF, Gage DJ, Cho YK and Shor LM (2018) Bacterial Extracellular Polymeric Substances Amplify Water Content Variability at the Pore Scale. Front. Environ. Sci. 6:93. doi: 10.3389/fenvs.2018.00093

INTRODUCTION

Soil microbes strongly influence the productivity and composition of terrestrial ecosystems. Microbes enhance nutrient acquisition by plants, protect plants from disease, and promote fertile, well-aggregated soils. (Barrios, 2007; van der Heijden et al., 2008). Extracellular polymeric substances (EPS) produced by soil bacteria can have a strong influence on soil moisture (Roberson and Firestone, 1992; Bais et al., 2006; Bengough, 2012; Adessi et al., 2018; Zheng et al., 2018). Plants also produce mucilage, a hydrogel similar to bacterial EPS in function. The production of hydrogels by plants and microbes contribute to the higher local water content typically found in the rhizosphere as compared with bulk soil. (Carminati et al., 2010; Moyano et al., 2013; Sadeghi et al., 2017; Aufrecht et al., 2018).

EPS promotes retention of soil moisture by at least three separate mechanisms. First, the EPS material holds moisture directly within its polymeric matrix. EPS swells and shrinks to remain saturated despite large changes in overall moisture content. As a result, organisms associated with EPS remain hydrated and maintain access to dissolved constituents (Or et al., 2007). Second, EPS promotes the formation of soil aggregates (Amellal et al., 1998; Godinho and Bhosle, 2009; Büks and Kaupenjohann, 2016; Lehmann et al., 2017). Small pores typical of intra-aggregate spaces hold water tightly, while the increased abundance of large, inter-aggregate macropores facilitates drainage, and therefore gas exchange (Donot et al., 2012; Castellane et al., 2014). Third, EPS on surfaces can modify water repellency of a soil, leading to more hydrophobic micropores that inhibit water evaporation (Ahmed et al., 2016; Cruz et al., 2017). Each of these mechanisms are discussed in more detail below.

The composition of bacterial EPS is highly dependent on bacterial species (Wingender et al., 2001; Vaningelgem et al., 2004; Schaumann et al., 2007; Mora et al., 2008) and the environmental conditions under which it is formed (McSwain et al., 2005; Zhang et al., 2014). EPS may be composed of some or all of the following: polysaccharides, proteins (both structural proteins and enzymes), extracellular DNA, lipids, and surfactants. The various components enable attachment to soil surfaces, immobilization and degradation of macromolecules for use by cells, and cell-cell communication (Flemming and Wingender, 2010). Of primary interest from a soil physics standpoint are hydrophilic exopolysaccharides such as alginate which are responsible for retention of water within the EPS matrix.

The physical and chemical microstructure of soil influences the spatial distribution of soil water. In a real aggregated soil, water tends to reside in intra-aggregate spaces where capillary forces are strongest (Albers, 2014; Sakai et al., 2015), while the larger pore spaces between aggregates are less likely to be saturated at a given matric potential. The addition of EPS has been shown to shift the water retention curve of sand or soil toward higher water contents (Chenu and Roberson, 1996; Rosenzweig et al., 2012), thereby modulating the effects of drying conditions on bacterial cells embedded in the EPS matrix.

Soil surface properties are also extremely important to soil moisture retention. The presence of hydrogels and organic matter can lead to a heterogeneous distribution of hydrophobic and hydrophilic surface chemistries. EPS produced by different bacteria was observed to either increase or decrease water repellency in incubated soil (Schaumann et al., 2007). Studies on mixed wettability (i.e., variable contact angle) in soil have shown that surface properties modulate evaporation in soil (Shokri et al., 2008). In prior work, we have shown that pore water is retained longer in micromodels with more hydrophobic surfaces compared with micromodels with identical physical geometries but more hydrophilic surfaces (Cruz et al., 2017).

In real soils, soil composition, physical structure and surface hydrophobicity vary simultaneously and the contributions of each can be difficult to decouple. To better understand the physical, chemical, and biological mechanisms contributing to microbial processes in soil we have developed emulated soil micromodels featuring a realistic sandy loam pore geometry. Deng et al. (2015) employed these experimental systems to demonstrate that a small amount of EPS produced by the soil bacterium *Sinorhizobium meliloti* acts with soil microstructure to inhibit evaporation of pore water. Later, Cruz et al. (2017) found that both aggregation state and surface wetting properties are important in pore-sale water dynamics: while surface hydrophobicity dominated pore structure in influencing the overall water evaporation rate, pore structure was key to the spatial distribution (i.e., hydraulic connectivity) of pore water, especially at intermediate saturations.

Microbes are dramatically affected by the physical and chemical properties of their microenvironment (Sheng et al., 2010; Colica et al., 2014; Harimawan and Ting, 2016). Meanwhile, microbes also have the power to alter key physical and chemical features of their microenvironment through the production of EPS. The microscale variability of real soil and the dynamic feedback between microbial processes and microscale environment features makes for a dauntingly complex system. Prior work has suggested that soil bacteria and bacterial EPS can act synergistically microscale physical features to inhibit water loss (Deng et al., 2015). It is unknown if a bacteria-free solution of EPS retains this moisture retaining function, or how EPS-mediated moisture retention is influenced by pore size.

The purpose of this study was to systematically measure EPS-mediated moisture retention for bacteria-free EPS solutions as a function of both EPS solution concentration and pore size. Emulated soil micromodels were employed to reproduce the realistic physical geometry of an aggregated sandy loam soil. We also evaluated EPS-mediated moisture retention in glass capillary tubes, representing a fine macropore regime, as well as in microfluidic capillary arrays, representing a micropore regime. Bacterial EPS solutions were prepared from EPS collected from the common soil bacterium *Sinorhizobium meliloti*. The well-described EPS structures, biosynthetic pathways, EPS mutants and sophisticated genetic tools make *S. meliloti* a useful species for these and future studies. We report that EPS concentration had no effect on pore water retention in the larger chambers with a diameter of 1.2 mm. However, in the experimental systems with pores in the micropore regime, EPS concentration had a

dramatic effect on all aspects of moisture retention. These results have important implications on elucidating the mechanisms of EPS-mediated moisture retention at the microscale and for better understanding and predicting overall function of the rhizosphere system.

MATERIALS AND METHODS

Chemicals

Granulated agar and biotin (99%) were purchased from Fisher BioReagents. $CaCl_2$, $CoCl_2$, KH_2PO_4, $MgSO_4$, NaCl, NH_4Cl, $C_4H_4O_4Na_2 \cdot 6H_2O$ were all ACS grade and purchased from Fisher Chemical. Na_2HPO_4 was USP grade and purchased from MP Biomedicals. Artificial groundwater salts including $CaSO_4$, KNO_3, KH_2PO_4, $MgSO_4$, NaCl, $NaHCO_3$ were all ACS grade and purchased from Fisher Chemical.

Preparation of EPS Solutions

EPS was produced by a model organism commonly found in the soil rhizosphere that is known to both fix nitrogen and produce EPS. *Sinorhizobium meliloti* strain Rm1021 is a quorum-sensing mutant with a natural insertion in *expR* that results in relatively low-level production of the exopolysaccharide galactoglucan (EPSII) (Pellock et al., 2002).

S. meliloti wild type strain Rm1021 was streaked onto M9 (0.2 $\mu g\ mL^{-1}$ biotin, 0.1 mM $CaCl_2$, 0.039 nM $CoCl_2$, 22 mM KH_2PO_4, 1 mM $MgSO_4$,40 mM Na_2HPO_4, 8.6 mM NaCl, 19 mm NH_4Cl, 0.2% succinate) agar and grown for 5 d at 30°C. Individual colonies were inoculated into 35 mL M9 media and incubated 5 d at 30°C and 300 rpm shaking. Aliquots were collected and compared to optical density of growth curves measured at 595 nm in 48 well plates (Synergy HT plate reader, BioTek, Winooski, VT) to confirm that cultures had reached stationary phase.

To harvest EPS, supernatant from stationary-phase cultures was collected by centrifugation (20 min, 2500 × g and 4°C) and filtered by 0.22-μm polyvinylidene fluoride (PVDF) syringe filters (Fisherbrand™ Syringe Filters) to produce so-called "1 × M9 EPS" solution (Alasonati and Slaveykova, 2012). This solution was diluted with 3 parts deionized (DI) water to produce "0.25 × M9 EPS" solution. Both of these solutions were used in the glass capillary and emulated soil micromodel experimental systems. The 1 × M9 EPS solution had a glucose-equivalent concentration of 58 $\mu g\ mL^{-1}$ via the anthrone-sulfuric acid assay (Morris, 1948; Mendis et al., 2016). To prepare the "5 × EPS" solution also used in the glass capillary experimental system, M9 EPS supernatant was re-suspended in aqueous ethanol solution (v/v = 75%) and dialyzed (Fisher brand Regenerated Cellulose Dialysis Tubing, 3500 Da, Fisher Scientific) against DI water for 5 d, then lyophilized (Savant™ SC210-115 SpeedVac system, Thermo Scientific) to remove excess water (González et al., 1996). This purified EPS solid was then dissolved in DI water. The glucose-equivalent concentration of this solution was 290 $\mu g\ mL^{-1}$ via the anthrone-sulfuric acid assay.

Since salt concentrations in these EPS solutions varied, solutions with different concentrations of EPS but uniform salt compositions were also prepared. Here, purified EPS solid was dissolved in artificial groundwater (AGW) to produce the "1 × EPS in AGW" (58 $mg\ L^{-1}$) and "5 × EPS in AGW" (290 $mg\ L^{-1}$) solutions used in the microcapillary array experimental system.

Experimental Systems

Three different experimental systems were used to measure EPS-mediated moisture retention as a function of pore size (**Table 1**). Glass capillary tubes with an inner diameter of 1.2 mm were used in both the Macropore Evaporative Flux Experiments and Macropore Drying Experiments (**Figure 1A**). This is the simplest experimental system where it is easy to quantify evaporation rate by the linear retreat of the air-water interface in systems large enough to see without magnification. Second, emulated soil micromodels were used in Soil Micromodel Drying Experiments to systematically control and exactly replicate a physical microstructure similar to an aggregated sandy loam soil (**Figure 1B**). Finally, microfluidic capillary arrays were used in in the Micropore Drying Experiments to measure EPS-mediated moisture retention in the micropore regime (**Figure 1C**). The details of each of these experiments and experimental systems are describe in further detail below.

Macropore Evaporative Flux Experiments

Pseudo steady state evaporative flux was measured for three different EPS solutions (0.25 × M9 EPS, 1 × M9 EPS, and 5 × EPS, see **Table 1**) in separate chambers at three RH values (nominally 42, 50, and 80%). Each humidity regime was established inside a separate round petri dish (Corning™ Falcon™ Bacteriological Petri Dishes with Lid) containing different amounts (2, 1, or 0 g) of $CaCl_2$. For each humidity value, 3 replicate capillary tubes were filled with each solution via 100-μL Eppendorf Pipette, then affixed to the bottom of the dish at 5 mm spacing in parallel orientation (9 capillaries per dish). Dishes were closed and the junction between top and bottom dishes was tightly wrapped with a double-layer of Scotch tape. The length of liquid remaining inside each capillary tube was recorded every few hours over 25 h using a digital microscope (Dino-Lite Edge Digital Microscope AM7115MZT, AnMo Electronics Corporation, Taiwan). The temperature and humidity sensor recorded the actual temperature and RH inside the chamber during the experiment. Chambers with target RH of 42, 50, and 80% were actually maintained at 46 ± 5.1%, 49 ± 4.2% and 80 ± 16.9% RH with corresponding temperatures of 24 ± 0.8, 24 ± 0.5 and 26 ± 0.6°C over the 25-h duration of the experiment.

We also measured the pseudo steady state evaporative flux of DI water at different relative humidities as a control. Here, 80 μL of sterile DI water was loaded into 1 mm diameter micro haematocrit capillary tubes (non-heparinized, Eisco Labs, Rochester, NY) using a pipette. Three filled capillary tubes were placed inside a large petri dish (Fisher Scientific, Hampton, NY), alongside three lengths of measuring tape to aid in tracking the progress of the air-water interface. In some cases, two 100-μL wells of saturated hygroscopic salt solution (KCl or Na_2HPO_4) were also placed inside the petri dish to maintain constant RH. Then dishes were closed and sealed with Scotch tape. The experiment was conducted at 4 RH values, with humidity

TABLE 1 | Summary of the different solutions used in each experiment including number of replicates across all relative humidity (RH) treatments.

Experiment Name	Solutions tested (total replicates)			
	Control	Low EPS	Medium EPS	High EPS
Macropore Evaporative Flux	DI Water (12)	0.25 × M9 EPS (9)[a]	1 × M9 EPS (9)[b]	5 × EPS (9)[c]
Macropore Drying	DI Water (3)	0.25 × M9 EPS (3)[a]	1 × M9 EPS (3)[b]	-
Soil Micromodel Drying	DI Water (18)	0.25 × M9 EPS (6)[a]	1 × M9 EPS (9)[b]	-
Micropore Drying	1 × AGW (54)[d] 5 × AGW (54)[e]	-	1 × EPS in AGW (54)[d]	5 × EPS in AGW (54)[d]

[a] *Salt composition: 0.25 × M9 media.*
[b] *Salt composition: 1 × M9 media.*
[c] *Salt composition: no salts; purified, solid EPS dissolved in deionized water.*
[d] *Salt composition: 1 × artificial groundwater.*
[e] *Salt composition: 5 × artificial groundwater.*

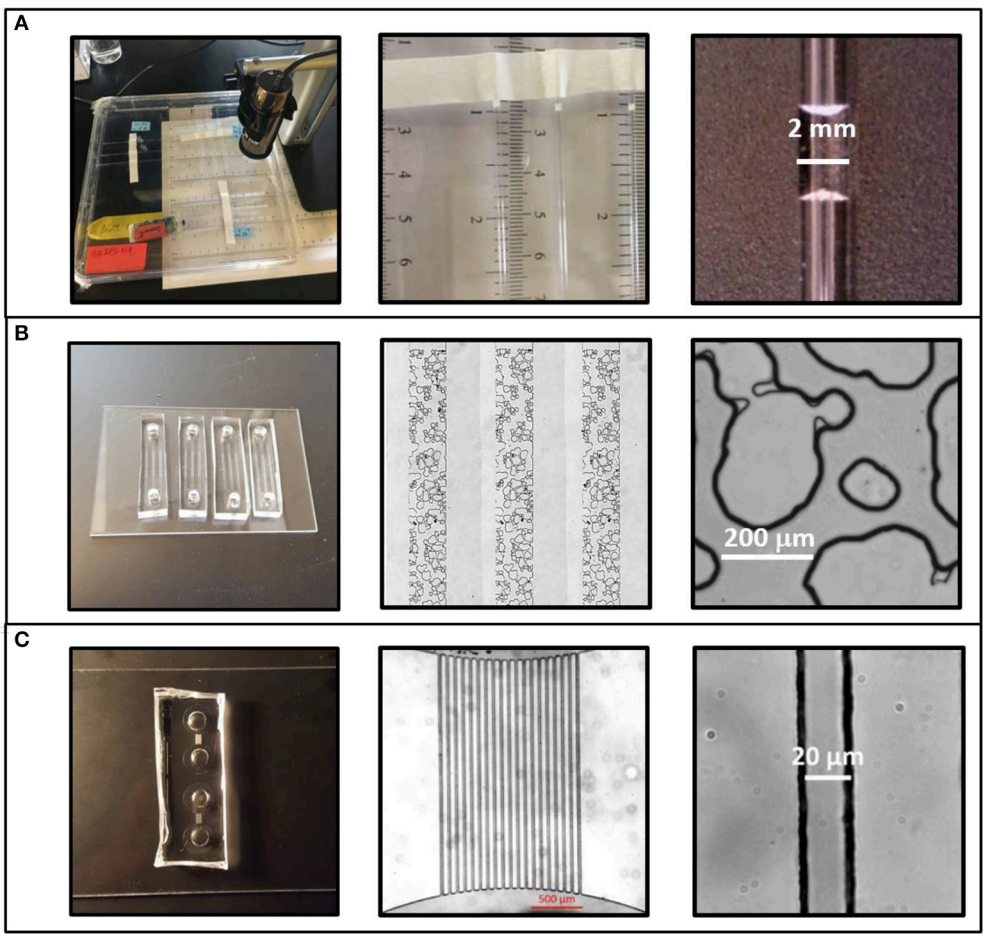

FIGURE 1 | Three experimental systems were used to test the effects of physical geometry on extracellular polymeric substance (EPS)-mediated drying behavior. **(A)** Intrinsic moisture retention behavior was measured in a macroscale regime using glass capillaries with an internal diameter of 1.2 ± 0.01 mm. **(B)** Drying behavior in soil-like geometries was measured using emulated soil micromodels. This systems features a 1 mm × 10 mm × 35 µm (w:l:h) microstructured region with a physical geometry similar to aggregated sandy loam soil. Pore widths range from 10 µm to >300 µm. **(C)** Microcapillary arrays were used for high-throughput determination of micropore regime effects. This system features bundles of 19 microchannels each measuring 20 µm × 34 µm × 2.2 mm (w:h:l).

control by different mechanisms: 42% (ambient lab RH), 95% (created with steam inside closed chamber), 85% (sealed petri dish with Na_2HPO_4), and 83% (sealed petri dish with KCl). For the DI water controls, the position of the air-water interface was recorded either by a programmed smartphone suspended above the petri dish (every half hour), or manually approximately every

TABLE 2 | Average water flux for evaporative flux experiments performed at (a) pseudo steady state of water at four different relative humidity (RH) and at (b) three different RH for each of three different EPS solutions.

Average RH (%, mean and standard deviation)	Solution	Average flux (mg mm^{-2} h^{-1})
42 ± 0.4	DI Water	2.50 ± 0.89
83 ± 1.0		0.69 ± 0.42
85 ± 0.6		0.41 ± 0.15
95 ± 0.9		0.29 ± 0.10
46 ± 5.1	0.25 × M9 EPS[a]	0.71 ± 0.34
	1 × M9 EPS[b]	0.69 ± 0.29
	5 × EPS[c]	0.82 ± 0.27
49 ± 4.2	0.25 × M9 EPS[a]	0.69 ± 0.25
	1 × M9 EPS[b]	0.66 ± 0.18
	5 × EPS[c]	0.72 ± 0.36
80 ± 16.9	0.25 × M9 EPS[a]	0.26 ± 0.15
	1 × M9 EPS[b]	0.28 ± 0.12
	5 × EPS[c]	0.25 ± 0.13

[a]*Salt composition: 0.25 × M9 media.*
[b]*Salt composition: 1 × M9 media.*
[c]*Salt composition: no salts; purified, solid EPS dissolved in deionized water.*

2 h, except overnight. Smartphone images were culled down to one image every 2 h and analyzed after the conclusion of the experiment. RH was monitored and observed to be consistent (±7%) during the time domain used to compute evaporative flux.

For all evaporative flux experiments, water flux from capillary tubes in mg mm^{-2} hr^{-1} was calculated based on the moving position of the air-fluid interface and the known time interval. Here, specific gravity of the solutions was assumed to be unity since the combined concentration of all solutes is $< <$ 1% by mass. Flux calculations excluded the initial phase and included the next 20-60 h, as data were available. Values of instantaneous flux were averaged over a 4-h timespan to reduce variability in the dataset.

Macropore Drying Experiments

The rate of water loss was measured from 100 to 0% saturation for three different solutions (0.25 × M9 EPS, 1 × M9 EPS, and DI water, see **Table 1**) at one RH, nominally 65%. Here, Kimax® melting point glass capillary tubes (34500–99, length = 100 mm, I.D.:1.2 ± 0.01 mm, or similar) were filled using a MicroFil syringe needle (MF34G-5, I.D. 100 μm, O.D. 164 μm), then affixed to the bottom of a 25 × 25 cm square petri dish (Corning™ Untreated 245 mm Square BioAssay Dishes) at 5 mm spacing. The dish was closed with a double-layer of Scotch tape, and the remaining liquid inside each capillary tube was measured and recorded every few days using a digital microscope (Dino-Lite Edge Digital Microscope AM7115MZT, AnMo Electronics Corporation, Taiwan) until the tube completely dried. Temperature and humidity were 22 ± 2.5°C and 66 ± 15%, respectively, for the 2-month duration of the experiment.

Soil Micromodel Drying Experiments

Emulated soil micromodels consist of three parallel microchannels each featuring an identical 1 mm × 10 mm × 35 μm (width, length, height) microstructured region (**Figure 1B**). The microstructured region featured a pseudo-2D geometry that represents a "slice" from a real sandy loam soil. Microchannel geometry was uniform with height. Plan dimensions of "pillars" and "gaps" emulate a realistic particle size distribution and pore size distribution of an aggregated sandy loam soil. Key features of the micromodels are (1) the realistic pore scale soil geometry, and (2) precise replication of the geometry from channel to channel and experiment to experiment, and (3) the ease of directly observing the progress of the air-water interface over time. See our prior work (Deng et al., 2015; Cruz et al., 2017; Soufan et al., 2018) for additional details on the creation, validation, and use of the aggregated sandy loam pseudo-2D soil geometry.

Microfluidic devices were fabricated using standard photolithography and soft lithography methods as described previously (Deng et al., 2013). Briefly, polydimethylsiloxane (PDMS, Sylgard 184, Dow Corning, Midland, MI), a two-part silicone elastomer, was cast over a photolithography master, then cured at 60°C for 6 h, then cut out using a scalpel and punched on both side using a 4-mm biopsy punch (Integra® Miltex). PDMS castings and glass slides were cleaned with isopropyl alcohol (99%, Fisher Chemical) and methanol (Laboratory Grade, Fisher Scientific), respectively, dried at 60 °C at least 1 h, then cooled to room temperature.

After 30 s treatment with oxygen plasma, microdevices were bonded to a clean glass slide then loaded immediately with 5 μL EPS solution using a pipette. Solutions were loaded into devices immediately after plasma bonding to ensure a consistently low water repellency in all experiments, corresponding to a water-air-PDMS contact angle of ∼8° (Cruz et al., 2017). The hydrophilic surface chemistry causes the fluid added in one well to immediately wick through the emulated soil micromodels. After devices were filled with solutions, the excess fluid was removed from the well region by pipette (Eppendorf 10-μL Pipette) and the microchannel remained full. Then, devices were placed and sealed inside the control chamber, and the infiltration of the air phase was imaged over time. Rate and extent of water loss was measured in emulated soil micromodels for two different solutions (0.25 × M9 EPS and 1 × M9 EPS, see **Table 1**) at a target RH of 75%. Drying behavior for the 0.25 × M9 EPS and 1 × M9 EPS solutions is also compared with DI water using data reported previously (Cruz et al., 2017).

Air infiltration was imaged over time throughout each microstructured region using an AxioObserver Z1 AX10 inverted wide field microscope (CarlZeiss, Oberkochen, Germany) using transmitted light and a 2.5 × objective corresponding with a field of view of ∼4 × 4 mm. Overlapping frames encompassing the entire microstructured region of each device were collected every 20 min for 3 d or longer (depending on the time required to reach 0% saturation or apparent equilibrium).

Soil micromodel drying experiments were performed inside a custom-built control chamber designed to maintain consistent RH on a microscope stage. Full details on the design and

operation of the control chamber apparatus are available elsewhere (Deng et al., 2015). Briefly, the control chamber was comprised of custom-milled plastic base with that fit snugly into the stage of an AxioObserver Z1 AX10 inverted wide field microscope (CarlZeiss, Oberkochen, Germany). A gasket-lined opening in the base enabled one or more glass slides to be firmly mounted directly above the microscope objectives. A gasket-lined lid of clear polycarbonate was mounted via thumb screws to the side walls of the control chamber's base creating an open space large enough to permit air flow inside the control chamber but small enough to fit below the condenser of the inverted microscope. A second large mixing chamber was connected to the control chamber via plastic tubing. The mixing chamber contained a cigar humidifier (Cigar Oasis, Farmingdale, NY) producing a RH of ∼75%. A MSR humidity sensor was placed inside the control chamber a few centimeters from the emulated soil micromodels to log both RH and temperature. The humidifier would be initiated at least 2 h prior to the start of each drying experiment to allow temperature and RH to equilibrate.

Image analysis followed a similar procedure as described previously (Cruz et al., 2017). Generally, mosaic images of the 1 mm × 1 cm microstructured region was converted into an 8-bit gray-scale image and thresholded by open source Fiji processing package ImageJ to resolve the continuous vapor interface along hydrated pore spaces or PDMS pillars (Schindelin et al., 2012). Then, the vapor area behind the vapor-liquid interface was manually filled with red pixels guided by the position of the vapor-liquid interface. Micromodel saturation (%) was calculated using the ratio of vapor area to total pore area:

$$Sat\ (\%) = (1 - \frac{A_V - A_C}{A_T - A_C}) \times 100\% \quad (1)$$

where Sat is saturation, A_V is the vapor-phase area, A_C is the area of the channel in each image outside the 1 mm × 1 cm microstructure region, and A_T is the total pore area in the micromodel.

The start of the experiment was operationally defined as the time when the air interface had just reached the start of the microstructured region on both sides of the channel. The end of the experiment was operationally defined as three consecutive hours with no discernable change in saturation (see Cruz et al., 2017).

Micropore Drying Experiments

The microfluidic capillary array is a separate PDMS-on-glass microfluidic device comprised of bundles of 19 parallel microchannels (each channel is 20-μm wide and 35-μm high) and each microchannel bundle connects two inlet/outlet wells. The device is an "array" because the wells are arranged in the footprint of a 48-well plate to facilitate loading with a multichannel pipette and data analysis using a plate reader. The length of individual microchannels varies slightly due to curvature of the wells and averaged 2.2 mm (**Figure 1C**). The design enables rapid determination of changing saturation for 19 separate microchannels loaded simultaneously with an identical solution. Saturation changes are measured in one dimension and is visible via microscope along the entire length of all microchannels in a bundle in a single field of view. Microcapillary array devices were produced using photolithography and soft lithography as described above.

The rate of pore water evaporation was measured in microcapillary arrays for five different solutions (5 × EPS in AGW, 1 × EPS in AGW, DI water, 1 × AGW, and 5 × AGW, see **Table 1**) at a target RH of 75%. Microcapillaries were loaded with each solution as described above. Excess fluid was removed from wells, then loaded devices were sealed inside the control chamber and the infiltration of air coupled with the evaporation of water from pores was imaged over time. Images were collected as above but at a magnification of 5 × and at a frequency of 1 min. Three replicates were performed for each solution. For each experiment, the time required to completely dry each of the 19 capillaries was recorded.

RESULTS AND DISCUSSION

Relation of Experimental Systems to Pore Regime

Three different experimental systems were employed to describe EPS-mediated moisture retention as a function of EPS concentration and pore size. The glass capillary tube experimental system is defined here as a bulk "macropore" regime by noting that pores >1,000 μm would be at least partially air-filled at a capillary pressure potential of −0.3 kPa. Field capacity (the degree of saturation after excess water has drained away) of soils ranges from about 8 to −10 kPa. Other prominent definitions for "macropore" include pores ≥ 1,000 μm (Luxmoore, 1981) or, alternatively, pores ≥ 75 μm (Brewer, 1965). These same authors define micropores as < 10 μm and <30 μm, respectively (**Table S1**). However, the most appropriate definition for macropore vs. micropore may be operational: Beven and Germann (1982) reviewed the topic and concluded that factors in addition to diameter such as pore connectivity determine preferential flow through soils.

In our simple system, bifurcated functionality from differences in structure can be understood by analyzing the differences in pore size distribution of our aggregated versus non-aggregated sandy loam emulated soil micromodel geometry (Cruz et al., 2017). The aggregated and non-aggregated micromodels have identical particle size distributions but different pore size distributions due to rearrangement of the "particles" in the photolithography mask used to create the microfluidic master. The non-aggregated geometry has a fairly uniform pore size distribution with no macropores (**Figure S1A**). By rearranging particles to create the aggregated structure, pores with diameter of 20–50 μm and pores with diameter of 200-240 μm were most increased, while pores with diameter of 60–140 μm were most decreased (**Figure S1A**). Based on the shape of the aggregated distribution we defined an operational micropore/macropore cutoff of 150 μm and fitted separate normal distributions to the pore size distributions. We find that the mean micropore is 44.8 ± 20.6 μm diameter, while the mean macropore is 212 ± 34.8 μm (**Figure S1B**). The sizes of our microfluidic capillary array (micropore regime) and glass capillary tube (macropore regime) experimental systems are consistent with these size domains.

Effect of EPS and RH on Evaporative Flux in the Macropore Regime

Evaporative flux was measured for DI water and EPS solutions in the glass capillary tube (macropore domain) experimental system. Sensitivity of evaporative flux to RH was also determined. RH was monitored throughout all evaporative flux experiments with mean and standard deviation for EPS solution evaporative flux experiment provided in **Table 2**. For the DI water experiments, RH was within ± 7% for all trials. For the EPS solution experiments, RH exhibited relatively high fluctuations. However, plotting flux against measured RH revealed there is little sensitivity of flux from EPS on RH (data not shown).

For DI water, evaporative flux ranged from 0.2 to 3.3 mg mm^{-2} hr^{-1}, depending on RH. For a given solution and RH value, evaporative flux was relatively constant over time (**Figure 2A**), indicating that a steady state was established within a few hours after drying began. Steady state fluxes for each replicate (with the initial transient values removed) were averaged together for further analysis. For DI water, the observed average evaporative flux was a strong function of RH (**Figure 2C**). The highest fluxes were observed for 42% RH, which was the driest experimental condition generated by the ambient cooling and air exchange system in the laboratory. Fluxes for 83, 85, and 95% RH were lower, with a sharp decrease in the differences between them as RH increased. Flux values were fitted with a natural log function of RH, with $R^2 = 0.99$.

For EPS solutions, evaporative flux varied from 0.1 to 1.5 mg mm^{-2} $h^{-1}$and exhibited a weaker dependence on RH than was observed for DI water (**Figures 2B,C**). EPS concentration had no obvious effect on magnitude of evaporative flux for a given RH. Averaged fluxes for the EPS solutions also exhibited a logarithmic dependence on RH, with $R^2 = 0.93$.

Evaporative flux from DI water or EPS solutions to the dryer air phase is dependent on the temperature of both phases (constant in our experiments), the saturation pressure of the liquid phase, and the vapor pressure in the gas phase (also dependent on the constant temperature) (Marek and Straub, 2001; Zhang et al., 2017). The pressures can be expressed as potentials, and the flux is proportional to the difference in water potential across the air-solution interface, with the magnitude determined by the transfer coefficient across the interface. The potential in the DI water phase is zero (fully saturated with no solute potential). The water potential in the air phase is given by Durner and Or (2005).

$$\psi_w = \frac{RT\rho_w}{M_w} \ln(RH) \quad (2)$$

Our results showing a logarithmic dependence of averaged fluxes on RH can be explained by Equation (2) above, with the EPS transfer coefficient value 2-4 times lower than that for DI water.

No Evidence for EPS-Mediated Moisture Retention in the Macropore Regime

The effect of EPS concentration on moisture retention in the macropore regime was measured using glass capillary tubes loaded with either DI water, 0.25 × M9 EPS, or 1 × M9 EPS held at 22 ± 2.5°C and at 66 ± 15% RH. Here, pore saturation (%) equals the length of the remaining water phase. In the initial stage of the drying process (0–15th day), all chambers exhibited rapid decline in saturation with little variance between replicates. From the 15 to 60th day, the drying rate declined slightly (**Figure 3A**) for all treatments, however at no point was there a statistically significant trend in the rate of moisture loss as a function of EPS concentration (Paired *t*-test, 2 tails: DIW vs. 0.25 × M9 EPS, $P = 0.98$; 0.25 × vs. 1 × M9 EPS, $P = 0.64$; DIW vs. 1 × M9 EPS, $P = 0.65$). All tubes reached 0% saturation on the 69th or 72nd day, with no statistically significant trend in the time required to reach 0% saturation among the treatments (unpaired *t*-test, 2 tails, equal variance: DIW vs. 0.25 × M9 EPS, $P = 1.0$; 0.25 × vs. 1 × M9 EPS, $P = 0.12$; DIW vs. 1 × M9 EPS, $P = 0.15$). Upon drying, the 0.25 × M9 EPS and the 1 × M9 EPS solutions left a clear white residue, corresponding to ∼0.19 and 0.22% of total capillary length, respectively. No residue was observed in the DI water capillaries, as expected.

These results show that EPS does not promote moisture retention in the macropore regime. All three solutions: 0.25 × M9 EPS and 1 × M9 EPS and DI water dried at the same rate and to the same extent.

Strong Evidence for EPS-Mediated Moisture Retention in Emulated Soil Micromodels

EPS-mediated moisture retention was also measured in emulated soil micromodels. For each experiment, two microfluidic devices each comprised of three microfluidic channels were filled with EPS solution, placed in the control chamber, and the infiltration of the air phase as pore water evaporated was imaged over time. Actual RH and temperature was 70 ± 2.5% (experiment with 0.25 × M9 EPS), 71 ± 1.3% (experiment with 1 × M9 EPS), and 76 ± 2.2% (additional experiment with 1 × M9 EPS).

In contrast with the results from the macropore drying experiments just discussed, in the emulated soil micromodels, EPS concentration clearly has a strong effect on the rate, on the extent, and on the variability of pore water retention (**Figure 3B**). Solutions identical to those used in the macropore drying experiments, above, now employed in a micropore regime slowed the drying rate by more than an order of magnitude compared with DI water. For example, in our previously-reported drying kinetics for DI water, the typical time for the saturation to drop below 50% was about 1 h (Cruz et al., 2017). The corresponding time for EPS solutions to drop below 50% saturation in similar emulated soil micromodels (same aggregated sandy loam geometry, same surface hydrophobicity) increased to about 8 h for the 0.25 × M9 EPS solution and to about 16 h for the 1 × M9 EPS solution (**Figure 3B**). Comparing the two EPS solutions, the drying rate slowed by a factor of 2. Chemically, the difference between the DI water and the 0.25 × M9 EPS solution are some simple salts and just 14.5 μg/ml glucose equivalent of EPS.

Perhaps even more important than the rate of water loss from a soil system is the quantity of water than can be held at a given

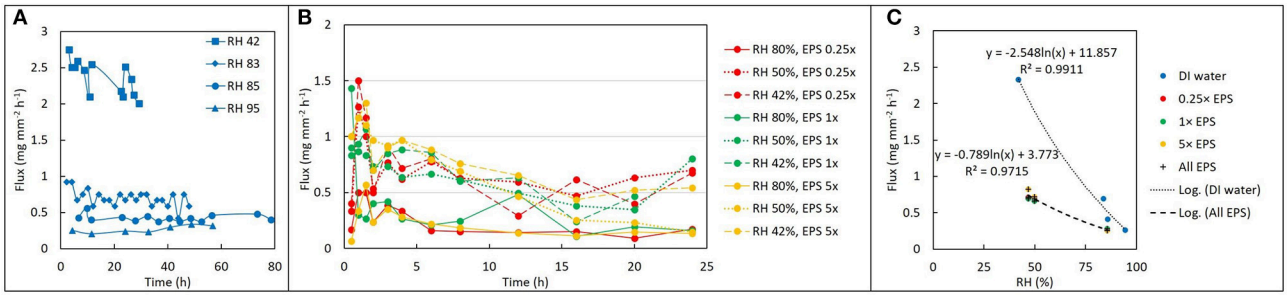

FIGURE 2 | Drying behavior as a function of EPS concentration and relative humidity (RH). **(A)** Change in water volume vs. time expressed as flux (mg mm^{-2} h^{-1}) for deionized water at four different values of RH. **(B)** Evaporative flux from different EPS solutions at different values of RH: after an initially higher rate, the flux becomes approximately constant over time. **(C)** Time-averaged flux decays exponentially with increase in RH for both water (blue) and EPS. Note that although concentration of EPS does not seem to influence the flux at a given RH, the difference between evaporative flux for EPS solutions versus deionized water varies by a factor of 2–4 times depending on RH.

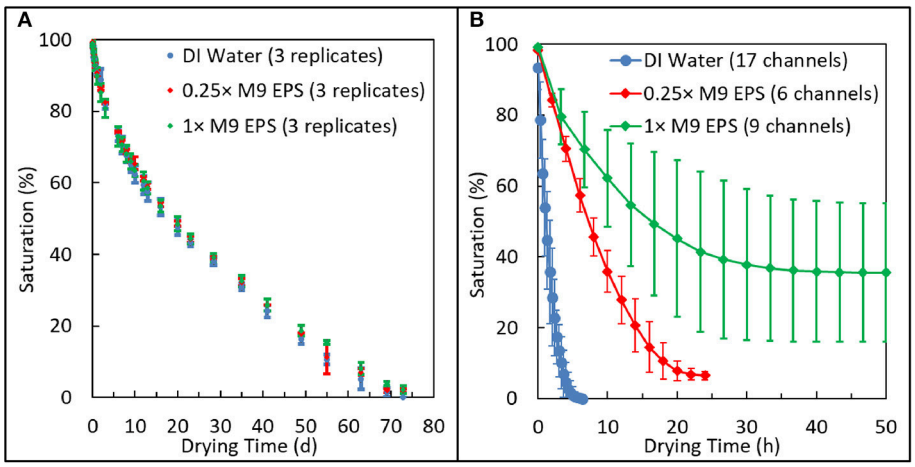

FIGURE 3 | Comparison of relative drying behavior of 1 × and 0.25 × extracellular polymeric substance (EPS) solutions suspened in M9 media at the macroscale and in an emulated soil geometry. **(A)** Glass capillary system shows all three solutions dried at similar rates and to similar extents in the macropore regime. **(B)** Emulated soil micromodel systems shows how EPS acts with microstructured physical geometry to dramatically reduce the rate and extent of drying and to enhance variability in pore-scale moisture retention.

matric potential. We define residual saturation as the saturation that persists in our experiments over time after the labile pore water has been evaporated. In similar emulated soil micromodels (same aggregated geometry, same surface hydrophobicity) at a similar RH, we previously reported a residual saturation for DI water of 0% for all 18 replicates (Cruz et al., 2017). However, with the addition of a small amount of EPS, residual saturation increased dramatically (**Figure 3B**). Average residual saturation was 6.4 ± 1.4% for the 0.25 × M9 EPS solution and 38 ± 19% for the 1 × M9 EPS solution (**Figure 3B**). Differences in residual saturation across treatments were highly significant (unpaired *t*-test, 2 tails, unequal variance: DIW vs. 0.25 × M9 EPS, $P < 0.0001$; 0.25 × vs. 1 × M9 EPS, $P < 0.001$; DIW vs. 1 × M9 EPS, $P < 0.001$). These results are further evidence that small amounts of EPS act together with a microscale pore structure to limit water evaporation at narrow pore throats (Deng et al., 2015).

EPS-Mediated Variation in Microscale Water Content

Together with influencing the rate and extent of water evaporation in the micropore regime, we find strong evidence that EPS concentration also influences the variability of residual saturation (**Figure 3B**). Recall that residual saturation was 0 ± 0% for DI water ($n = 18$), while residual saturation ranged from 4.7 to 8.5% for the 0.25 × M9 EPS solution ($n = 6$) and from 15 to 74% for the 1 × M9 EPS solution (n=9). The difference in sample variance between the two EPS solution treatments was highly significant ($F = 183$, $P < 0.000001$).

Variability of residual saturation may be best understood by examining the time course of air infiltration within individual emulated soil micromodel channels. Time series of mosaic images of individual channels shows the air interface becomes "stuck" in certain positions and that this significantly impacts saturation (see **Videos V1-V6** provided in the Supplementary

Information). For example, representative mosaic images at 0, 20, and 40 h for three replicates channels loaded with the 1 × M9 EPS solution shows the air interface began at approximately the same position in all cases: flush with the "soil" structures to the left and right and just starting to infiltrate into the large central "macropore" (**Figure 4A**). However, 20 h later, Channel 1 and Channel 3 are at very nearly the same saturation of about 60% with nearly identical positions of the air-water interface, while progress of air infiltration of Channel 2 seems to be lagging well behind. These same trends can be seen graphically in the plot of saturation for these channels versus time (**Figure 4B**). At 40 h, not much additional progression on the right side of Channel 2 is observed, but infiltration has continued on the left side of Channel 2. In contrast, no infiltration on the left is observed in Channels 1 and 3, while progression from the right is observed in Channels 1 and 3. Channel 1 experiences the greatest degree of air infiltration, achieving a saturation of ∼40% by 40 h compared with about 52 and 54%, respectively for Channels 3 and 2. The corresponding RH and temperature are provided in **Figure 4C**.

Although all channels exhibit similar invasion-percolation behavior as expected in emulated soil micromodels, and as observed previously (Deng et al., 2015; Cruz et al., 2017), there is substantial variation in the progression of water evaporation. Also, unlike in our prior work (Deng et al., 2015), variability cannot be attributed to potential biological growth or redistribution of bacteria in the device because here we are using a cell-free purified EPS suspension. We conclude that a combination of high interfacial velocity causing unsteady Haines jumps (Cruz et al., 2017) and solution properties of the EPS itself are contributing to this variability observed only in the micropore regime.

High-Throughput Investigation of EPS-Mediated Moisture Retention in the Micropore Regime

The soil micromodel drying experiments described above require several weeks to complete, including somewhat laborious image processing. To enhance uniformity and throughput, a microfluidic capillary array device was employed to quickly measure EPS-mediated drying resistance in the micropore regime in dozens of small capillaries simultaneously. Here, microcapillary devices were loaded with four different solutions and held at 75% RH. To avoid confounding factors from EPS and salts concentrations varying simultaneously, here, solutions with different concentrations of EPS were prepared from a salt-free lyophilized solid dissolved into a constant artificial groundwater (AGW) salt solution, as described earlier. Microcapillary drying of these 5 × and 1 × EPS in AGW solutions was also compared with 1 × and 5 × AGW alone (i.e., AGW and concentrated AGW with no EPS) to better understand the effects of salts versus EPS in mediating micropore regime drying resistance. Three replicate experiments were completed. In each replicate experiment, four separate microcapillary devices were each loaded with different solutions: 5 × EPS in AGW, 1 × EPS in AGW, 1 × AGW, or 5 × AGW. The actual RH and temperature in replicate experiments was 75 ± 1.6%, 77 ± 0.9%, and 79 ± 1.3% and 23 ± 0.6°C, 23 ± 0.5°C, 23 ± 0.4°C, respectively.

Here, the time required to dry the entire channel was recorded from examination of microscope images collected of each microcapillary bundle every 1 min. Different EPS solutions (0×, 1 × and 5 × EPS all in 1 × AGW) dried in 22 ± 7 min, 37 ± 11 min, and 56 ± 20 min (**Figure 5**). Differences in drying time are statistically significant (Unpaired *t*-test, 2 tails, unequal variance: 1 × EPS vs. 0× EPS, $P < 0.000001$; 5 × EPS vs. 1 × EPS, $P < 0.000001$; 5 × EPS vs. 0× EPS, $P < 0.000001$). With higher EPS content but identical salt, the variance in drying time between these treatments increased as well. (1 × EPS vs. 0× EPS, $F = 171$, $P < 0.01$; 5 × EPS vs. 1 × EPS, $F = 171$, $P < 0.0001$; 5 × EPS vs. 0× EPS, $F = 171$, $P < 0.00001$.)

We also compared microcapillary drying time for different salt concentrations that contained no EPS. The drying time of 1 × and 5 × AGW solutions were similar and averaged 26 ± 9 min and 24 ± 10 min, respectively (**Figure S2**). There is no statistically significant difference in drying time as a function of salt concentration. There is a statistically significant difference in drying time as a function of EPS concentration.

In examining the drying time by channel, it seems apparent that the edge channels dried faster (**Figure 5**). Indeed, an analysis of relative drying rates across by channel shows that the 2 edge channels dry significantly faster than the others (data not shown). However, by pairing the data by channel and RH then comparing across solution treatments, the effect of solution type on drying time is easily determined despite variability among individual channels.

Interactions Among EPS, Salts, and Microstructure

Studies measuring evaporation of saline water from porous geometries are common in several fields, including environmental, agricultural, and engineering applications (El-Dessouky et al., 2002; Fujimaki et al., 2006). Pore structure is known to strongly influence the evaporation rate of water from soil (Norouzi Rad and Shokri, 2012; Shokri-Kuehni et al., 2017). We have shown that EPS dramatically inhibits the rate and extent of moisture loss and enhances variability of moisture content at the micropore scale. Our microfluidic capillary experiments definitively show that salts alone do not inhibit moisture loss at the micropore scale. However, salts are important for the proper function of EPS at the pore scale. As water evaporates, the local EPS and salt concentrations will be simultaneously increased, especially near the air-fluid interface. The resulting higher concentration of EPS and salt may affect the moisture distribution within the porous structure. Ionic polysaccharides are likely to interact with cations in groundwater especially divalent cations such as Ca^{2+} to form a cross-linked hydrogel structure that strongly retains moisture via hydrogen bonding and hydrophilic interactions (Fringant et al., 1996).

Both rate of water loss and the spatial distribution of water in a microenvironment are important to the function of soil systems. Rate of water loss will control the overall saturation of a soil as it dries after a rain event, while spatial distribution

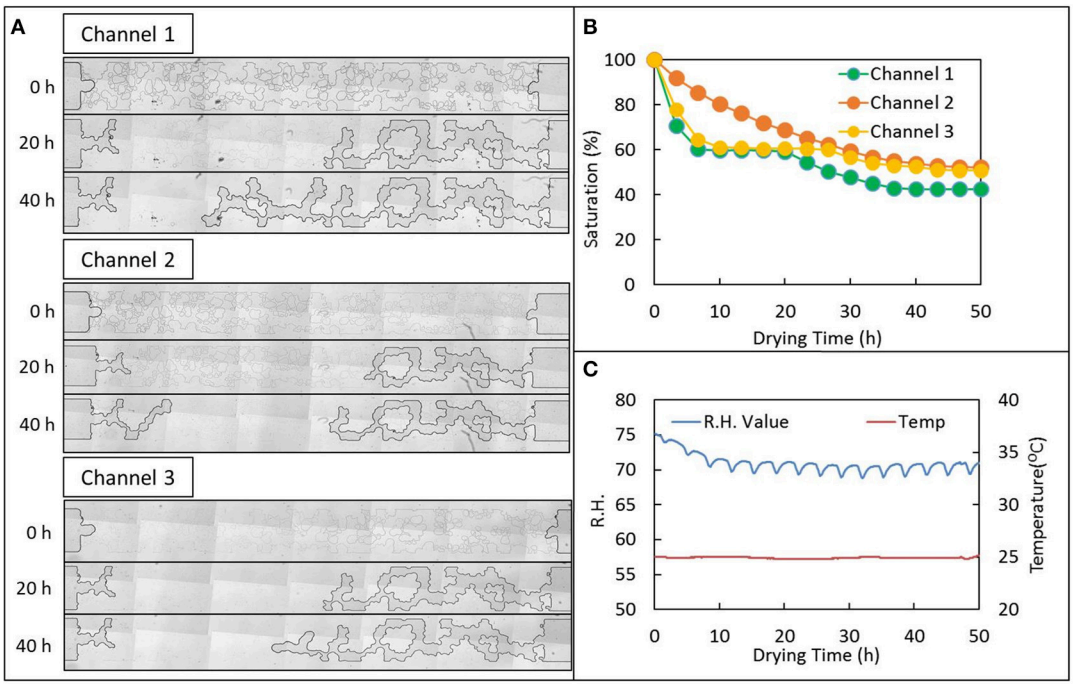

FIGURE 4 | Drying behavior of a 1 × extracellular polymeric substance (EPS) solution suspended M9 media loaded into an emulated soil micromodel geometry and held at 70-75% relative humidity (RH). **(A)** Tiled mages of individual replicate micromodel channels (see **Figure 1B**) at the operationally-defined start of the drying experiment and 20 and 40 h later. **(B)** Fraction of water remaining (saturation) for the same channels as in **(A)** vs. time. **(C)** RH and temperature recorded in the control chamber via USB recorder for the data shown in **(A,B)**. See **Supplemental Information** for movies of drying behavior.

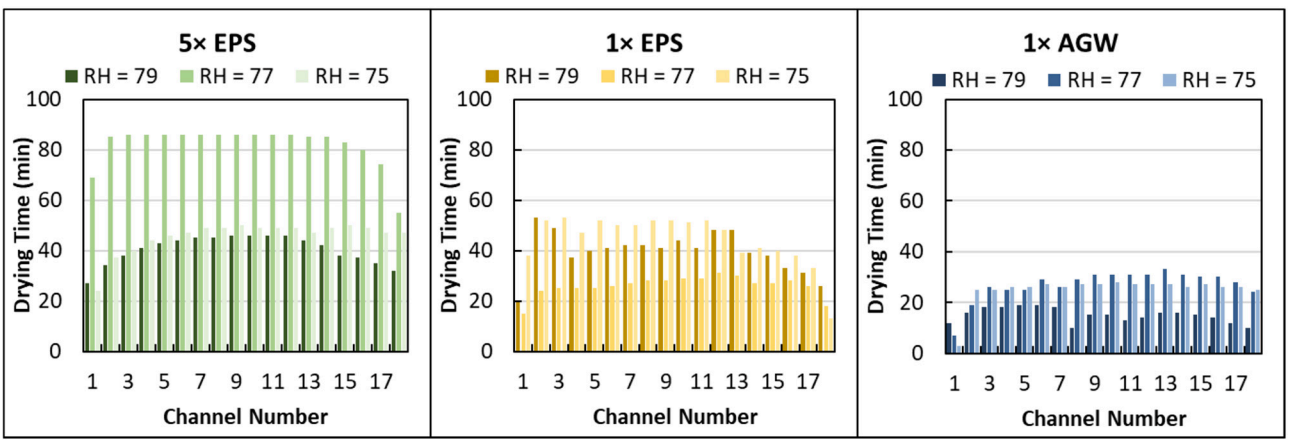

FIGURE 5 | Drying time distribution for different concentration extracellular polymeric substance (EPS) solutions suspended in artificial groundwater (AGW) in microcapillary arrays at different relative humidity (RH). Data are shown for 5 × EPS in 1 × AGW, 1 × EPS in 1 × AGW, and 1 × AGW (no EPS) at 79, 77, and 75% RH.

will determine proximity to soluble constituents in the aqueous (saturated) regions and proximity to gaseous constituents in the unsaturated regions. Position of water can therefore control whether aerobic or anaerobic conditions dominate, and if soils are net producers of greenhouse gasses. For example, Owens et al., estimated that pores <26.8 μm diameter remained full at a field potential of −11 kPa, which could lead to the creation of anaerobic microsites and influence overall N_2O production (Owens et al., 2017). Microscale spatial and temporal variability of water distribution conditions is also a major factor driving diversity in soil microbial communities. Studies under a range of *in-situ* and experimental conditions have shown that hydraulic isolation caused by fragmentation of the water phase leads to higher bacterial diversity and richness (Zhou et al., 2002; Treves et al., 2003; Carson et al., 2009; Chau et al., 2011). Taxa that might otherwise compete for resources

are sequestered in disconnected water films in unsaturated soil, allowing them to coexist, but not compete, in very small volumes.

The mechanism for EPS enhancement of moisture content variability is not yet clear. One possibility is that a pore-clogging mechanism related to the precipitation of EPS or the formation of a local skin-like structure bridging narrow pore throats is responsible for reducing local water flux to near zero. Obtaining proof of this physical configuration in dilute, hydrated EPS systems is an analytical challenge. However, others have employed advanced technology, e.g., ToF-SIMS, NMR, and electron microscopy to probe the composition and microstructure of EPS within biofilms *in situ* (Marshall et al., 2006; Dohnalkova et al., 2011; Renslow et al., 2017) and found evidence for EPS structures such as fibers which could potentially reduce the water flux through the EPS matrix.

CONCLUSION

The inherent complexity of the rhizosphere makes for a fascinating system for study (Aleklett et al., 2017; Anbari et al., 2018; Borer et al., 2018). Emulated soil micromodels employed here offer complex yet reproducible and realistic physical pore geometries and the opportunity to directly observe microscale phenomena to enhance functional understanding of the soil system. In this study, relatively small quantities of EPS were found to dramatically affect drying behavior within emulated soil micromodels and at the micropore scale (but not at the macropore scale).

Soils at an intermediate saturation tend to be the most productive (Bouman and Tuong, 2001). Such soils have a mixture of water and gas-filled pore spaces, enabling organisms in soil to access both dissolved and gaseous substrates (Smith et al., 2003). The potential for EPS to *not* impede water evaporation from macropores at higher saturations yet strongly inhibit evaporation in a concentration-dependent fashion as the smaller pores empty at lower saturations is a remarkable microscale microbial process of the natural soil system. This functionality clearly promotes maintenance of the maximally-productive intermediate saturation condition over time.

Another key finding of this report is the enhancement in local variability of moisture content with EPS concentration. Taxa that might otherwise compete for resources are sequestered in disconnected water films in unsaturated soil, allowing them to coexist, but not directly compete, in very small volumes. This could be a mechanism by which alpha diversity (in-site diversity) is maintained or enhanced in soil or the rhizosphere at larger scales, while enhancing beta diversity (between-site diversity) on the pore scale. Thus, enhanced variability of moisture, driven by bacterial synthesis of EPS, may lead to greater diversity of microbial communities and therefore greater resiliency of terrestrial ecosystems (Griffiths and Philippot, 2013). Testing the hypothesis that water film disconnections enhance these diversity indices will require careful, controlled studies and emulated soil micromodels may prove useful for such work.

AUTHOR CONTRIBUTIONS

Y-SG, JF, DG, YC, and LS created the overall concept and experiment design. Y-SG and AK designed and fabricated microfluidic devices. Y-SG, HH, and JF acquired primary data, and Y-SG, JF, and LS analyzed the data and drafted the manuscript. All authors discussed the results and contributed to the final manuscript.

ACKNOWLEDGMENTS

All data which support the conclusions presented in this manuscript can be obtained from the corresponding author (leslieshor@gmail.com). To our knowledge there are no conflicts of interest. We are grateful to Daniel Dougherty, Daniel Zeigher, and Wallis (Will) Boyd for assistance with data collection and analysis. This work was supported by DOE award DE-SC0014522 and NSF award 1137249.

SUPPLEMENTARY MATERIAL

The Supplementary Material for this article can be found online at: https://www.frontiersin.org/articles/10.3389/fenvs.2018.00093/full#supplementary-material

Figure S1 | Pore size distribution of **(A)** aggregated and non-aggregated micromodel **(B)** aggregated micromodel pore geometries showing the bimodal normal distribution for miropores and macropores.

Figure S2 | Drying time distribution for 5 × AGW and 1 × AGW in microcapillary arrays at different relative humidity.

Table S1 | Summary of the experiments and experimental systems described in this report.

Videos V1–V6 | Air infiltration into individual emulated soil micromodel channels initially saturated with dilute extracellular polymeric substance (EPS) solutions suspended in M9 media.

REFERENCES

Adessi, A., de Carvalho, R. C., De Philippis, R., Branquinho, C., and da Silva, J. M. (2018). Microbial extracellular polymeric substances improve water retention in dryland biological soil crusts. *Soil Biol. Biochem.* 116, 67–69. doi: 10.1016/j.soilbio.2017.10.002

Ahmed, M. A., Kroener, E., Benard, P., Zarebanadkouki, M., Kaestner, A., and Carminati, A. (2016). Drying of mucilage causes water repellency in the rhizosphere of maize: measurements and modelling. *Plant Soil* 407, 161–171. doi: 10.1007/s11104-015-2749-1

Alasonati, E., and Slaveykova, V. I. (2012). Effects of extraction methods on the composition and molar mass distributions of exopolymeric substances of the bacterium *Sinorhizobium meliloti*. *Bioresour. Technol.* 114, 603–609. doi: 10.1016/j.biortech.2012.03.071

Albers, B. (2014). Modeling the hysteretic behavior of the capillary pressure in partially saturated porous media: a review. *Acta Mech.* 225, 2163–2189. doi: 10.1007/s00707-014-1122-4

Aleklett, K., Kiers, E. T., Ohlsson, P., Shimizu, T. S., Caldas, V. E., and Hammer, E. C. (2017). Build your own soil: exploring microfluidics to create microbial habitat structures. *ISME J.* 12, 312–319. doi: 10.1038/ismej.2017.184

Amellal, N., Burtin, G., Bartoli, F., and Heulin, T. (1998). Colonization of wheat roots by an exopolysaccharide-producingpantoea agglomerans strain and its effect on rhizosphere soil aggregation. *Appl. Environ. Microbial.* 64, 3740–3744.

Anbari, A., Chien, H.-T., Datta, S. S., Deng, W., Weitz, D. A., and Fan, J. (2018). Microfluidic model porous media: fabrication and applications. *Small* 14, 1703575–1703515. doi: 10.1002/smll.201703575

Aufrecht, J. A., Timm, C. M., Bible, A., Morrell-Falvey, J. L., Pelletier, D. A., Doktycz, M. J., et al. (2018). Microfluidics: quantifying the spatiotemporal dynamics of plant root colonization by beneficial bacteria in a microfluidic habitat (Adv. Biosys. 6/2018). *Adv. Biosys.* 2:1870051. doi: 10.1002/adbi.201800048

Bais, H. P., Weir, T. L., Perry, L. G., Gilroy, S., and Vivanco, J. M. (2006). The role of root exudates in rhizosphere interactions with plants and other organisms. *Annu. Rev. Plant Biol.* 57, 233–266. doi: 10.1146/annurev.arplant.57.032905.105159

Barrios, E. (2007). Soil biota, ecosystem services and land productivity. *Ecol. Econ.* 64, 269–285. doi: 10.1016/j.ecolecon.2007.03.004

Bengough, A. G. (2012). Water dynamics of the root zone: rhizosphere biophysics and its control on soil hydrology. *Vadose Zone J.* 11:vzj2011.0111. doi: 10.2136/vzj2011.0111

Beven, K., and Germann, P. (1982). Macropores and water flow in soils. *Water Resour. Res.* 18, 1311–1325. doi: 10.1029/WR018i005p01311

Borer, B., Tecon, R., and Or, D. (2018). Spatial organization of bacterial populations in response to oxygen and carbon counter-gradients in pore networks. *Nat. Commun.* 9:769. doi: 10.1038/s41467-018-03187-y

Bouman, B., and Tuong, T. P. (2001). Field water management to save water and increase its productivity in irrigated lowland rice. *Agric. Water Manag.* 49, 11–30. doi: 10.1016/S0378-3774(00)00128-1

Brewer, R. (1965). Fabric and mineral analysis of soils. *Soil Sci.* 100:73.

Büks, F., and Kaupenjohann, M. (2016). Enzymatic biofilm digestion in soil aggregates facilitates the release of particulate organic matter by sonication. *SOIL* 2, 499–509. doi: 10.5194/soil-2-499-2016

Carminati, A., Moradi, A. B., Vetterlein, D., Vontobel, P., Lehmann, E., Weller, U., et al. (2010). Dynamics of soil water content in the rhizosphere. *Plant Soil* 332, 163–176. doi: 10.1007/s11104-010-0283-8

Carson, J. K., Campbell, L., Rooney, D., Clipson, N., and Gleeson, D. B. (2009). Minerals in soil select distinct bacterial communities in their microhabitats. *FEMS Microbiol. Ecol.* 67, 381–388. doi: 10.1111/j.1574-6941.2008.00645.x

Castellane, T. C. L., Lemos, M. V. F., and de Macedo Lemos, E. G. (2014). Evaluation of the biotechnological potential of rhizobium tropici strains for exopolysaccharide production. *Carbohydr. Polym.* 111, 191–197. doi: 10.1016/j.carbpol.2014.04.066

Chau, J. F., Bagtzoglou, A. C., and Willig, M. R. (2011). The effect of soil texture on richness and diversity of bacterial communities. *Environ. Forensics* 12, 333–341. doi: 10.1080/15275922.2011.622348

Chenu, C., and Roberson, E. B. (1996). Diffusion of glucose in microbial extracellular polysaccharide as affected by water potential. *Soil Biol. Biochem.* 28,1–8. doi: 10.1016/0038-0717(96)00070-3

Colica, G., Li, H., Rossi, F., Li, D., Liu, Y., and De Philippis, R. (2014). Microbial secreted exopolysaccharides affect the hydrological behavior of induced biological soil crusts in desert sandy soils. *Soil Biol. Biochem.* 68, 62–70. doi: 10.1016/j.soilbio.2013.09.017

Cruz, B. C., Furrer, J. M., Guo, Y. S., Dougherty, D., Hinestroza, H. F., Hernandez, J. S., et al. (2017). Pore-scale water dynamics during drying and the impacts of structure and surface wettability. *Water Resour. Res.* 53, 5585–5600. doi: 10.1002/2016WR019862

Deng, J., Dhummakupt, A., Samson, P. C., Wikswo, J. P., and Shor, L. M. (2013). Dynamic dosing assay relating real-time respiration responses of *Staphylococcus Aureus* biofilms to changing microchemical conditions. *Anal. Chem.* 85, 5411–5419. doi: 10.1021/ac303711m

Deng, J., Orner, E. P., Chau, J. F., Anderson, E. M., Kadilak, A. L., Rubinstein, R. L., et al. (2015). Synergistic effects of soil microstructure and bacterial EPS on drying rate in emulated soil micromodels. *Soil Biol. Biochem.* 83, 116–124. doi: 10.1016/j.soilbio.2014.12.006

Dohnalkova, A. C., Marshall, M. J., Arey, B. W., Williams, K. H., Buck, E. C., and Fredrickson, J. K. (2011). Imaging hydrated microbial extracellular polymers: comparative analysis by electron microscopy. *Appl. Environ. Microbiol.* 77, 1254–1262. doi: 10.1128/AEM.02001-10

Donot, F., Fontana, A., Baccou, J. C., and Schorr-Galindo, S. (2012). Microbial exopolysaccharides: main examples of synthesis, excretion, genetics and extraction. *Carbohydr. Polym.* 87, 951–962. doi: 10.1016/j.carbpol.2011.08.083

Durner, W., and Or, D. (2005). "Soil water potential measurement," in *Encyclopedia of Hydro- logical Sciences, Chapter 73*, eds M. G. Anderson and J. J. McDonnell (Chichester, UK: John Wiley and Sons, Ltd.), 1089–1102. doi: 10.1002/0470848944.hsa077a

El-Dessouky, H. T., Ettouney, H. M., Alatiqi, I. M., and Al-Shamari, M. A. (2002). Evaporation rates from fresh and saline water in moving air. *Indus. Eng. Chem. Res.* 41, 642–650. doi: 10.1021/ie010327o

Flemming, H.-C., and Wingender, J. (2010). The biofilm matrix. *Nat. Pub. Group* 8, 623–633. doi: 10.1038/nrmicro2415

Fringant, C., Desbrières, J., Milas, M., Rinaudo, M., Joly, C., and Escoubes, M. (1996). Characterisation of sorbed water molecules on neutral and ionic polysaccharides. *Int. J. Biol. Macromol.* 18, 281–286. doi: 10.1016/0141-8130(95)01087-4

Fujimaki, H., Shimano, T., Inoue, M., and Nakane, K. (2006). Effect of a salt crust on evaporation from a bare saline soil. *Vadose Zone J.* 5, 1246–1211. doi: 10.2136/vzj2005.0144

Godinho, A. L., and Bhosle, S. (2009). Sand aggregation by exopolysaccharide-producing microbacterium arborescens–AGSB. *Curr. Microbiol.* 58, 616–621. doi: 10.1007/s00284-009-9400-4

González, J. E., Reuhs, B. L., and Walker, G. C. (1996). Low molecular weight EPS II of Rhizobium meliloti allows nodule invasion in *Medicago sativa*. *Proc. Natl. Acad. Sci. U.S.A.* 93, 8636–8641. doi: 10.1073/pnas.93.16.8636

Griffiths, B. S., and Philippot, L. (2013). Insights into the resistance and resilience of the soil microbial community. *FEMS Microbiol. Rev.* 37, 112–129. doi: 10.1111/j.1574-6976.2012.00343.x

Harimawan, A., and Ting, Y.-P. (2016). Investigation of extracellular polymeric substances (EPS) properties of *P. aeruginosa* and *B. subtilis* and their role in bacterial adhesion. *Colloids Surf. B Biointerfaces* 146, 459–467. doi: 10.1016/j.colsurfb.2016.06.039

Lehmann, A., Zheng, W., and Rillig, M. C. (2017). Soil biota contributions to soil aggregation. *Nat. Ecol. Evol.* 1, 1828–1835. doi: 10.1038/s41559-017-0344-y

Luxmoore, R. J. (1981). Micro-, meso-, and macroporosity of soil. *Soil Sci. Soc. Am. J.* 45, 671–672. doi: 10.2136/sssaj1981.03615995004500030051x

Marek, R., and Straub, J. (2001). Analysis of the evaporation coefficient and the condensation coefficient of water. *Int. J. Heat Mass Trans.* 44, 1–15. doi: 10.1016/S0017-9310(00)00086-7

Marshall, M. J., Beliaev, A. S., Dohnalkova, A. C., Kennedy, D. W., Shi, L., Wang, Z., et al. (2006). c-Type cytochrome-dependent formation of U(IV) nanoparticles by *Shewanella oneidensis*. *PLoS Biol.* 4:e268–e210. doi: 10.1371/journal.pbio.0040268

McSwain, B. S., Irvine, R. L., Hausner, M., and Wilderer, P. A. (2005). Composition and distribution of extracellular polymeric substances in aerobic flocs and granular sludge. *Appl. Environ. Microbiol.* 71, 1051–1057. doi: 10.1128/AEM.71.2.1051-1057.2005

Mendis, H. C., Madzima, T. F., Queiroux, C., and Jones, K. M. (2016). Function of succinoglycan polysaccharide in sinorhizobium meliloti host plant invasion depends on succinylation, not molecular weight. *mBio* 7:e00606–16–11. doi: 10.1128/mBio.00606-16

Mora, P., Rosconi, F., Franco Fraguas, L., and Castro-Sowinski, S. (2008). *Azospirillum brasilense* Sp7 produces an outer-membrane lectin that specifically binds to surface-exposed extracellular polysaccharide produced by the bacterium. *Arch. Microbiol.* 189, 519–524. doi: 10.1007/s00203-007-0343-5

Morris, D. L. (1948). Quantitative determination of carbohydrates with dreywood's anthrone reagent. *Science* 107, 254–255. doi: 10.1126/science.107.2775.254

Moyano, F. E., Manzoni, S., and Chenu, C. (2013). Responses of soil heterotrophic respiration to moisture availability: an exploration of processes and models. *Soil Biol. Biochem.* 59, 72–85. doi: 10.1016/j.soilbio.2013.01.002

Norouzi Rad, M., and Shokri, N. (2012). Nonlinear effects of salt concentrations on evaporation from porous media. *Geophys. Res. Lett.* 39:L04403. doi: 10.1029/2011GL050763

Or, D., Phutane, S., and Dechesne, A. (2007). Extracellular polymeric substances affecting pore-scale hydrologic conditions for bacterial activity in unsaturated soils. *Vadose Zone J.* 6, 298–298. doi: 10.2136/vzj2006.0080

Owens, J., Clough, T. J., Laubach, J., Hunt, J. E., and Venterea, R. T. (2017). Nitrous oxide fluxes and soil oxygen dynamics of soil treated with cow urine. *Soil Sci. Soc. Am. J.* 81, 289–210. doi: 10.2136/sssaj2016.09.0277

Pellock, B. J., Teplitski, M., Boinay, R. P., Bauer, W. D., and Walker, G. C. (2002). A LuxR homolog controls production of symbiotically active extracellular polysaccharide ii by *Sinorhizobium meliloti*. *J. Bacteriol.* 184, 5067–5076. doi: 10.1128/JB.184.18.5067-5076.2002

Renslow, R. S., Marshall, M. J., Tucker, A. E., Chrisler, W. B., and Yu, X.-Y. (2017). *In situ* nuclear magnetic resonance microimaging of live biofilms in a microchannel. *Analyst* 142, 2363–2371. doi: 10.1039/C7AN00078B

Roberson, E. B., and Firestone, M. K. (1992). Relationship between desiccation and exopolysaccharide production in a soil *Pseudomonas sp*. *Appl. Environ. Microbiol.* 58, 1284–1291.

Rosenzweig, R., Shavit, U., and Furman, A. (2012). Water retention curves of biofilm-affected soils using xanthan as an analogue. S*oil Sci. Soc. Am. J.* 76, 61–69. doi: 10.2136/sssaj2011.0155

Sadeghi, S. H., Kheirfam, H., Homaee, M., Darki, B. Z., and Vafakhah, M. (2017). Improving runoff behavior resulting from direct inoculation of soil micro-organisms. *Soil Tillage Res.* 171, 35–41. doi: 10.1016/j.still.2017.04.007

Sakai, M., Van Genuchten, M. T., Alazba, A. A., Setiawan, B. I., and Minasny, B. (2015). A complete soil hydraulic model accounting for capillary and adsorptive water retention, capillary and film conductivity, and hysteresis. *Water Resour. Res.* 51, 8757–8772. doi: 10.1002/2015WR017703

Schaumann, G. E., Braun, B., Kirchner, D., Rotard, W., Szewzyk, U., and Grohmann, E. (2007). Influence of biofilms on the water repellency of urban soil samples. *Hydrol. Process.* 21, 2276–2284. doi: 10.1002/hyp.6746

Schindelin, J., Arganda-Carreras, I., Frise, E., Kaynig, V., Longair, M., Pietzsch, T., et al. (2012). Fiji: an open-source platform for biological-image analysis. *Nat. Methods* 9, 676–682. doi: 10.1038/nmeth.2019

Sheng, G.-P., Yu, H.-Q., and Li, X.-Y. (2010). Extracellular polymeric substances (EPS) of microbial aggregates in biological wastewater treatment systems: a review. *Biotechnol. Adv.* 28, 882–894. doi: 10.1016/j.biotechadv.2010.08.001

Shokri, N., Lehmann, P., and Or, D. (2008). Effects of hydrophobic layers on evaporation from porous media. *Geophys. Res. Lett.* 35, L19407-1–L19407-4. doi: 10.1029/2008GL035230

Shokri-Kuehni, S. M. S., Vetter, T., Webb, C., and Shokri, N. (2017). New insights into saline water evaporation from porous media: complex interaction between evaporation rates, precipitation, and surface temperature. *Geophys. Res. Lett.* 44, 5504–5510. doi: 10.1002/2017GL073337

Smith, K. A., Ball, T., Conen, F., Dobbie, K. E., Massheder, J., and Rey, A. (2003). Exchange of greenhouse gases between soil and atmosphere: interactions of soil physical factors and biological processes. *Eur. J. Soil Sci.* 54, 779–791. doi: 10.1046/j.1351-0754.2003.0567.x

Soil Science Society of America (2008). *Glossary Of Soil Science Terms*. Madison, WI: ASA-CSSA-SSSA.

Soufan, R., Delaunay, Y., Vieublé, L., Shor, L., Garnier, P., Otten, W., et al. (2018). Pore-scale monitoring of the effect of microarchitecture on fungal growth in a two-dimensional soil-like micromodel. *Front. Environ. Sci.* 6:68. doi: 10.3389/fenvs.2018.00068

Treves, D. S., Xia, B., Zhou, J., and Tiedje, J. M. (2003). A two-species test of the hypothesis that spatial isolation influences microbial diversity in soil. *Microb. Ecol.* 45, 20–28. doi: 10.1007/s00248-002-1044-x

van der Heijden, M. G. A., Bardgett, R. D., and van Straalen, N. M. (2008). The unseen majority: soil microbes as drivers of plant diversity and productivity in terrestrial ecosystems. *Ecol. Lett.* 11, 296–310. doi: 10.1111/j.1461-0248.2007.01139.x

Vaningelgem, F., Zamfir, M., Mozzi, F., Adriany, T., Vancanneyt, M., Swings, J., et al. (2004). Biodiversity of exopolysaccharides produced by streptococcus thermophilus strains is reflected in their production and their molecular and functional characteristics. *Appl. Environ. Microbiol.* 70, 900–912. doi: 10.1128/AEM.70.2.900-912.2004

Wingender, J., Strathmann, M., Rode, A., Leis, A., and Flemming, H.-C. (2001). "Isolation and biochemical characterization of extracellular polymeric substances from Pseudomonas aeruginosa," in *Methods in Enzymology*, ed R. J. Doyle (San Diego, CA: Elsevier; Academic Press), 302–314. doi: 10.1016/S0076-6879(01)36597-7

Zhang, L., Li, Y. R., Zhou, L. Q., and Wu, C. M. (2017). Comparison study on the calculation formula of evaporation mass flux through the plane vapour-liquid interface. *J. Phys. Conf. Ser.* 925, 012019–012017. doi: 10.1088/1742-6596/925/1/012019

Zhang, P., Fang, F., Chen, Y.-P., Shen, Y., Zhang, W., Yang, J.-X., et al. (2014). Composition of EPS fractions from suspended sludge and biofilm and their roles in microbial cell aggregation. *Chemosphere* 117, 59–65. doi: 10.1016/j.chemosphere.2014.05.070

Zheng, W., Zeng, S., Bais, H., LaManna, J. M., Hussey, D. S., Jacobson, D. L., et al. (2018). Plant Growth-Promoting Rhizobacteria (PGPR) reduce evaporation and increase soil water retention. *Water Resour. Res.* 178, 821–815. doi: 10.1029/2018WR022656

Zhou, J., Xia, B., Treves, D. S., Wu, L. Y., Marsh, T. L., O'Neill, R. V., et al. (2002). Spatial and resource factors influencing high microbial diversity in soil. *Appl. Environ. Microbiol.* 68, 326–334. doi: 10.1128/AEM.68.1.326-334.2002

Conflict of Interest Statement: The authors declare that the research was conducted in the absence of any commercial or financial relationships that could be construed as a potential conflict of interest.